ISME Communications, 2026, 6(1), ycag293
https://doi.org/10.1093/ismeco/ycag293
Published: 12 October 2026
Original Article
Editor's Choice

Genome-resolved analysis of an H_2-rich serpentinite enrichment identifies *Meiothermus* as a potential heterotroph for cell-derived substrate use

Sota Ihara[1,2,3], Hayate Hirai[4,5,6], Ryosuke Nakai[7], Hideyuki Tamaki[6,8,*], Akihiro Okamoto[2,3,8,9,10,*]

[1]Graduate School of Science and Technology, University of Tsukuba, 1-1-1 Tennodai, Tsukuba 305-8572, Japan
[2]International Center for Materials Nanoarchitectonics (WPI-MANA), National Institute for Materials Science, 1-1 Namiki, Tsukuba 305-0044, Japan
[3]Research Center for Macromolecules and Biomaterials, National Institute for Materials Science, 1-1 Namiki, Tsukuba 305-0044, Japan
[4]School of Life Science and Technology, Institute of Science Tokyo, 2-12-1 Ookayama, Meguro, Tokyo 152-8550, Japan
[5]Earth-Life Science Institute, Institute of Future Science, Institute of Science Tokyo, 2-12-1 I7E Ookayama, Meguro, Tokyo 152-8550, Japan
[6]Biomanufacturing Process Research Center (BPRC), National Institute of Advanced Industrial Science and Technology (AIST), 1-1-1 Higashi, Tsukuba, Ibaraki 305-8566, Japan
[7]Biomanufacturing Process Research Center (BPRC), National Institute of Advanced Industrial Science and Technology (AIST), 2-17-2-1, Tsukisamu-Higashi, Sapporo 062-8517, Japan
[8]Graduate School of Life and Environmental Science, University of Tsukuba, 1-1-1 Tennodai, Tsukuba 305-8577, Japan
[9]Graduate School of Chemical Sciences and Engineering, Hokkaido University, North 13 West 8, Kita-ku, Sapporo, 060-8628, Japan
[10]Research Center for Autonomous Systems Materialogy, Institute of Integrated Research, Institute of Science Tokyo (Science Tokyo), Yokohama, Kanagawa 226-8503, Japan

*Corresponding authors: Hideyuki Tamaki, Biomanufacturing Process Research Center (BPRC), National Institute of Advanced Industrial Science and Technology (AIST), 1-1-1 Higashi, Tsukuba, Ibaraki 305-8566, Japan. E-mail: tamaki-hideyuki@aist.go.jp; Akihiro Okamoto, Research Center for Macromolecules and Biomaterials, National Institute for Materials Science, 1-1 Namiki, Tsukuba, Ibaraki 305-0044, Japan. E-mail: OKAMOTO.Akihiro@nims.go.jp.

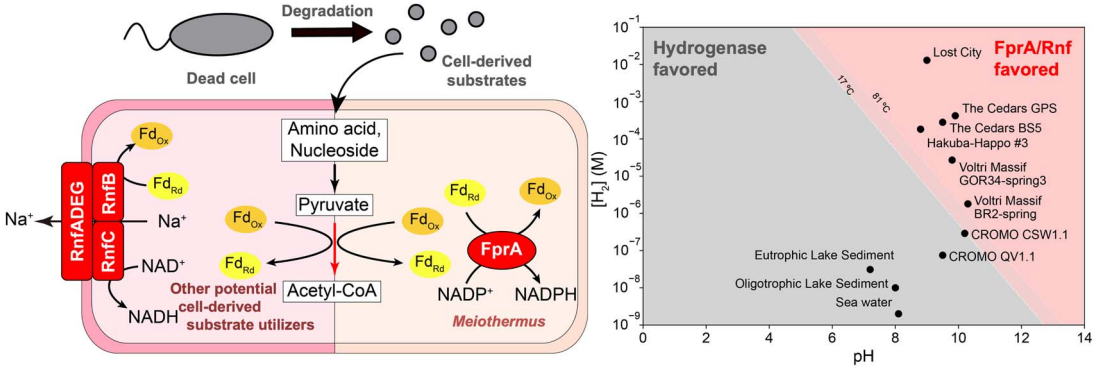
Abstract

Serpentinite-hosted ecosystems have been widely studied as analogues of early Earth environments, with particular emphasis on H_2-fueled lithoautotrophy. However, the ecological roles of heterotrophic microorganisms that utilize cellular biomass in these energy-limited systems remain poorly understood. Here, we report the reproducible enrichment of the genus *Meiothermus* during substrate-free incubation of biomass-concentrated fluids from the Hakuba–Happo serpentinite-hosted system. A high-quality *Meiothermus* metagenome-assembled genome encoded extracellular proteases, peptide and nucleoside transporters, and catabolic pathways for channeling cell-derived substrates into central metabolism. The genome further encoded both aerobic respiratory capacity and a putative acetate-forming fermentation pathway coupled to hydrogen-independent ferredoxin reoxidation, providing a thermodynamically plausible mechanism for ATP generation during amino acid degradation under H_2-rich, anoxic conditions. Notably, an acetate-forming fermentation module was restricted to serpentinite-derived *Meiothermus* lineages, consistent with possible habitat-associated metabolic differentiation within the genus. Extending beyond Hakuba–Happo, comparative analysis of 331 metagenome-assembled genomes from 15 datasets spanning six serpentinite-hosted systems identified diverse candidate lineages encoding gene complements consistent with cell-derived substrate catabolism and non-H_2-evolving ferredoxin oxidation modules, most frequently the Na^+-translocating Rnf complex. These findings expand the lithoautotrophy-centered view of serpentinite-hosted ecosystems by highlighting necromass-utilizing heterotrophs as potential contributors to carbon turnover and community persistence in deep, energy-limited biospheres.

Received: 6 July 2026. **Revised:** 8 September 2026. **Accepted:** 8 October 2026
© The Author(s) 2026. Published by Oxford University Press on behalf of the International Society for Microbial Ecology.
This is an Open Access article distributed under the terms of the Creative Commons Attribution License (https://creativecommons.org/licenses/by/4.0/), which permits unrestricted reuse, distribution, and reproduction in any medium, provided the original work is properly cited.

Downloaded from academic.oup.com/ismecommun/article/6/1/ycag293/8907494 by NATIONAL INSTITUTE FOR MATERIALS SCIENCE user on 18 November 2026

Graphical abstract



Keywords serpentinite system, *Meiothermus*, necromass utilization, genome-resolved metagenomics, ultra micro-area filtration

Introduction

Microbial communities persist through continuous turnover of biomass, a substantial fraction of which becomes necromass, such as dead cells, cellular debris, and extracellular macromolecules, that can be reutilized by other microorganisms [1–5]. Necromass recycling therefore represents a foundational process sustaining ecosystem function over long timescales and is likely to have played an important role since early stages of evolution, particularly in energy- and nutrient-limited settings [6].

However, necromass recycling is expected to be strongly constrained under conditions of limited terminal electron acceptors and high hydrogen availability, as postulated for some early Earth scenarios. Prokaryotic biomass is highly enriched in proteins, making amino acids the dominant potential substrates during necromass degradation [7, 8]. In many anaerobic microorganisms, amino acid catabolism relies on fermentative redox balancing that ultimately channels electrons to proton reduction, resulting in H_2 production [9, 10]. Classic studies of amino acid fermenting bacteria demonstrated that elevated H_2 partial pressures thermodynamically inhibit anaerobic amino acid catabolism, and that removal of H_2, either experimentally or through syntrophic association with hydrogen-consuming partners, can substantially enhance these processes [11–13]. Collectively, these observations predict that heterotrophic utilization of proteinaceous necromass should be unfavorable in environments where H_2 accumulates and terminal electron acceptors are scarce.

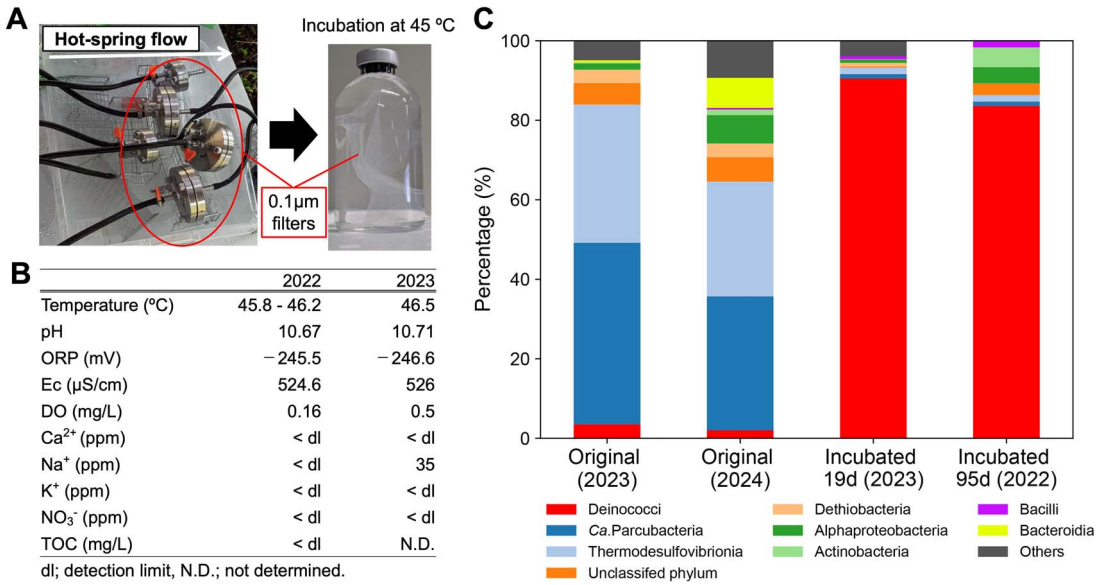
For many years, free hydrogen in the subsurface was assumed to be negligible, based on the expectation that it would be rapidly consumed and therefore not persist at high concentrations [14]. This view has been revised by accumulating evidence that H_2 can be continuously generated through multiple geochemical processes [14, 15]. Among these, serpentinization is thought to contribute substantially to global H_2 production and gives rise to serpentinite-hosted aquatic systems characterized by persistently high H_2 concentrations—often orders of magnitude greater than those found in typical surface environments [16]. These systems provide natural laboratories for investigating microbial ecology under chronic H_2 excess and limited availability of strong terminal electron acceptors. In parallel, increasing support for hypotheses linking the emergence of early life to H_2-rich water–rock reaction settings further motivates efforts to understand the metabolic constraints and solutions for microbial life under such conditions [17–19].

To date, research on semi-closed serpentinite-hosted systems with minimal external nutrient input has focused predominantly on hydrogen-oxidizing lithoautotrophs as primary producers, whereas the ecology of heterotrophic microorganisms has received comparatively little attention [20–23]. This imbalance likely reflects the prevailing expectation that anaerobic heterotrophy, particularly amino acid catabolism, should be thermodynamically constrained in hydrogen-rich, electron-acceptor-limited environments. Although this view is consistent with reports of low microbial abundances in many serpentinizing fluids relative to other aquatic environments [24, 25], it remains difficult to reconcile with the long-term persistence and stability of diverse microbial communities in serpentinite systems, where both external organic inputs and concentrations of dissolved inorganic carbon are extremely limited and overall primary productivity is expected to be low [19, 24].

Previous studies provide clues toward resolving this contradiction. Microbial communities attached to solid surfaces in serpentinite-hosted environments, such as mineral pores and fracture walls, can form localized microhabitats with cell densities up to four orders of magnitude higher than those in surrounding fluids [26]. Under such high-density and substrate-limited (starvation) conditions, microorganisms have been reported to upregulate molecular capacities for amino acid utilization and to preferentially assimilate substrates derived from dead cells [27–29], suggesting that necromass can become a significant resource within dense microbial assemblages.

We therefore hypothesized that heterotrophic microorganisms capable of utilizing necromass can be selectively enriched under biomass-concentrated conditions in serpentinite-hosted systems, and that such organisms may possess metabolic strategies enabling anaerobic utilization of protein- and nucleic-acid-derived substrates without net coupling to H_2 production. To test this hypothesis, we combined enrichment cultivation of microbial communities from the Hakuba–Happo hot spring, a serpentinite-hosted hydrothermal system in Japan, with comparative metagenomic analyses of serpentinite-hosted systems. Our results indicate that hydrogen-independent ferredoxin reoxidation routes are broadly distributed among candidate necromass-utilizing microorganisms, providing

Downloaded from academic.oup.com/ismecommun/article/6/1/ycag293/8907494 by NATIONAL INSTITUTE FOR MATERIALS SCIENCE user on 18 November 2026



	2022	2023
Temperature (°C)	45.8 - 46.2	46.5
pH	10.67	10.71
ORP (mV)	−245.5	−246.6
Ec (μS/cm)	524.6	526
DO (mg/L)	0.16	0.5
Ca^{2+} (ppm)	< dl	< dl
Na^{+} (ppm)	< dl	35
K^{+} (ppm)	< dl	< dl
NO_3^{-} (ppm)	< dl	< dl
TOC (mg/L)	< dl	N.D.

dl; detection limit, N.D.; not determined.

Figure 1 Biomass-concentrated incubation drives reproducible community shifts at the Hakuba–Happo #3 serpentinization site. (A) Workflow from field sampling to incubation. Hot-spring water was continuously filtered through a 0.1-μm pore-size filter to capture and concentrate microorganisms. Filters were transferred into vials containing site spring water and incubated at 45°C. (B) Geochemical parameters of Hakuba–Happo #3 measured in 2022 and 2023. Detection limits: 4 ppm for Ca^{2+}, 2 ppm for Na^{+}, 4 ppm for K^{+}, 6 ppm for NO_3^{-}, and 3 mg/L for TOC. (C) 16S rRNA gene-based community composition of the original environment and enrichment cultures after 19 and 95 days of incubation. Original environmental samples were collected in 2023 and 2024. The 19-day incubation sample derived from the 2023 incubation, and the 95-day incubation sample from the 2022 incubation.

a potential mechanism for sustaining heterotrophic metabolism in hydrogen-rich environments.

Materials and methods

Sampling, geochemical analysis, and incubation of concentrated serpentinite microorganisms

Microbial samples were collected from Hakuba–Happo #3 spring water (36°42' N 137°48' E, Nagano, Japan) in November 2022, July 2023, and October 2024, as described previously [23]. Continuous filtration through 0.1-μm pore-size filters yielded estimated enrichments of 3898-fold (2022) and 1418-fold (2023) over *in situ* cell densities, assuming complete cell retention and filter immersion in spring-water-filled vials (Fig. 1A). To minimize oxygen exposure, vials were vigorously flushed for ~10 s with H_2-rich spring water (flow rate not measured) and sealed without headspace after filter insertion. Samples from 2022 and 2023 were incubated at 45°C for 95 and 19 days, respectively. After incubation, cells were detached from filters by sonication (38 kHz, 240 W, 2 min; USL-400, SND Co. Ltd, Nagano, Japan) and vortexing (1 min; Vortex-Genie 2, Scientific Industries, NY, USA) for further analysis. Sampling and geochemical methods are detailed in Supplementary Methods.

Microbiome analysis

DNA from spring-water filters was extracted using Lysing Matrix E (MP Biomedicals, CA, USA) and DNeasy UltraClean Microbial Kit (Qiagen, Hilden, Germany). The 16S rRNA gene V4 region was amplified using the U515F/U805R primers. DNA from incubation samples was extracted using the ZymoBIOMICS DNA Miniprep Kit (Zymo Research, CA, USA) with bead beating, and the V4 region was amplified using the 515F/806R primers. Libraries were sequenced on MiSeq system (2 × 300-bp paired-end reads). Reads were processed in QIIME2 and representative sequences classified using SILVA. Library preparation and sequence processing are detailed in Supplementary Methods.

TEM observation following ultra micro-area filtration

For each incubation sample (6 days in 2023 or 95 days in 2022), 5 ml was mixed with an equal volume of 4% paraformaldehyde in 0.1 M cacodylate buffer (pH 10.0) that had been purged with N_2 for 30 min, and fixed for 1 h at room temperature. A total of 10 ml of fixed sample was filtered through a 4 mm-diameter area using the EZ-Fit™ Manifold base (Merck Co., Darmstadt, Germany) onto a 0.1 μm pore-size, 25 mm-diameter polyethersulfone (PES) membrane filter (AS ONE, Osaka, Japan) to achieve sufficient cell density for microscopic observation (Fig. 2A–C). The concentrated cells via ultra micro-area filtration (UMAF) on the filter were fixed overnight at 4°C using 2% glutaraldehyde in 0.05 M cacodylate buffer (pH 7.4), followed by conventional transmission electron microscopy (TEM) sample preparation and observation as described in the Supplementary Methods.

Genome-resolved metagenomic analysis

Genomic DNA from the 95-day incubation was amplified using the REPLI-g Single Cell Kit (Qiagen) because its concentration was below detection. After amplification according to the manufacturer's protocol, DNA was quantified using the Qubit™ dsDNA HS assay kit (Thermo Fisher Scientific, MA, USA). Metagenome processing, binning, and annotation are detailed in Supplementary Methods. Metagenomes retrieved from the NCBI Sequence Read Archive (SRA; Supplementary Table 1) were assembled as described previously [23].

Genome-based phylogenetic analysis

Single-copy housekeeping genes were extracted and aligned using GTDB-Tk version 2.4.0. Alignments were trimmed using trimAl ver.

Downloaded from academic.oup.com/ismecommun/article/6/1/ycag293/8907494 by NATIONAL INSTITUTE FOR MATERIALS SCIENCE user on 18 November 2026

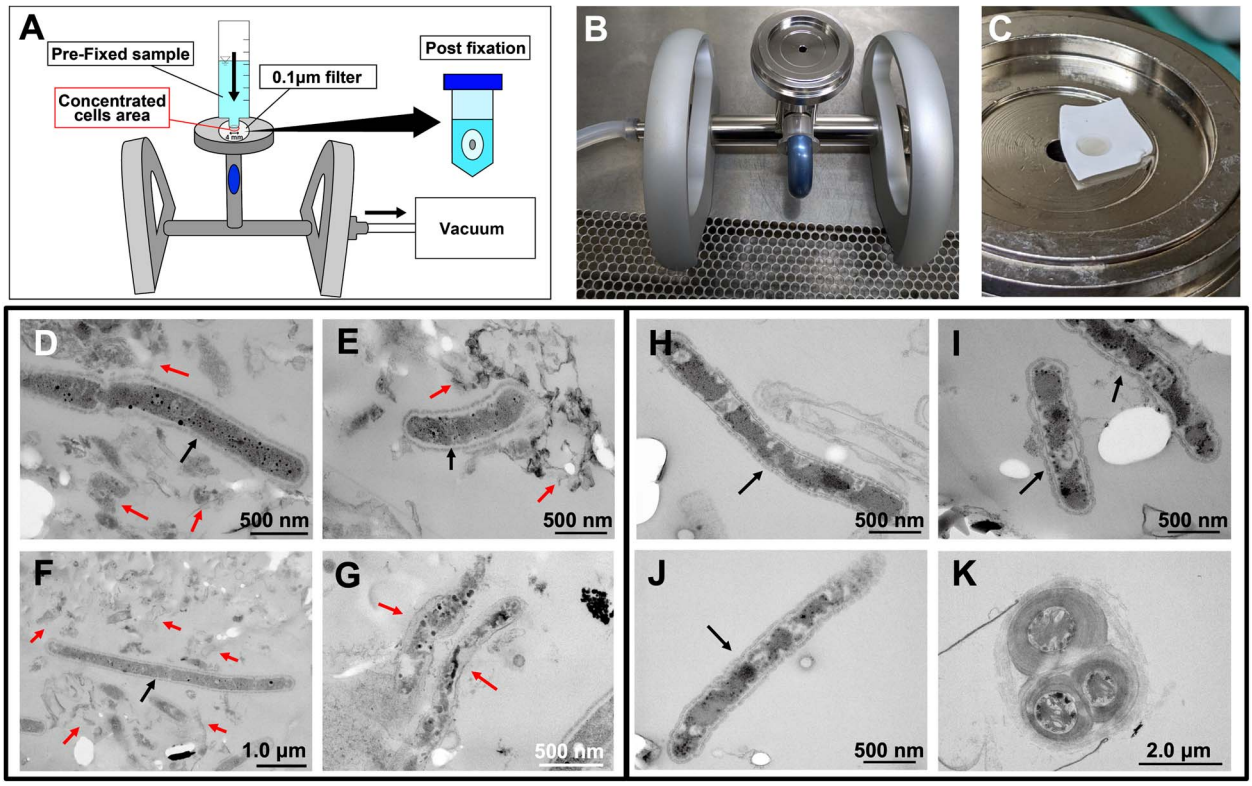


Figure 2 UMAF-based concentration enables TEM imaging from extremely low-biomass enrichment samples. (A) Schematic overview of the UMAF-based concentration workflow. Five milliliters of incubated sample were mixed 1:1 with 4% paraformaldehyde in 0.1 M cacodylate buffer (pH 10.0) for pre-fixation and loaded onto a syringe placed on a 0.1-μm PES filter mounted on an EZ-Fit manifold; subsequent fixation and staining were performed as described in Materials and methods section. Cells were concentrated onto a 4-mm-diameter micro-area by vacuum suction (≈40-fold increase in areal cell density). The filter was further fixed with 2% glutaraldehyde in 0.05 M cacodylate buffer (pH 7.4). (B) Photograph of the EZ-Fit™ manifold base used for micro-area suction. (C) Representative filter after concentrating the 95-day incubation sample; brown particulates likely reflect co-concentrated iron oxides from the spring water. (D–K) TEM micrographs of enrichment cultures incubated for 6 days (D–G) and 95 days (H–K) using samples collected in 2023 and 2022, respectively. Black arrows indicate the dominant *Meiothermus*-like rod-shaped cells; red arrows indicate cellular debris. (K) Sporangium-like structure with a thick, Gram-positive-like cell envelope. Scale bars are shown in each panel.

1.5.0 with automated trimming option (-automated1) [30]. A maximum likelihood phylogenetic tree was then constructed with IQ-TREE2 ver. 2.3.6, using the LG+F+G4 substitution model and performing 1000 ultrafast bootstrap replicates (-B 1000) and 1000 SH-like approximate likelihood ratio tests (-alrt 1000) [31].

Thermodynamic calculations

Gibbs free-energy (ΔG) changes were calculated for three ferredoxin-reoxidation reactions: hydrogenase-mediated ferredoxin oxidation with H_2 production, and NAD^+- and $NADP^+$-linked ferredoxin oxidation. Calculations were based on redox potentials and the Nernst equation, incorporating temperature, pH, and dissolved H_2 concentrations reported for serpentinite-hosted systems. Constants, standard redox potentials, environmental parameters, and reaction equations are provided in Supplementary Tables 2 and 3 and the Supplementary Methods.

Results

Microbiome shift during enrichment under high-biomass conditions

The Hakuba–Happo #3 serpentinization site has previously been reported to exhibit stable geochemistry and a consistent microbial community profile [21]. We first assessed temporal stability of the filter-retained microbiome over 2 years using 16S rRNA gene amplicon sequencing. In 2023, Ca. Parcubacteria and the class *Thermodesulfovibrionia* accounted for 80.4% of the community, and these same lineages remained dominant in 2024 (63.7%). In contrast, the class *Deinococci* represented a minor fraction in both years (3.5% in 2023 and 2.0% in 2024), indicating that the community was dominated by similar major taxa across years.

We also compared the geochemical profiles of Hakuba–Happo #3 measured in 2022 and 2023 (Fig. 1B). Although dissolved oxygen and sodium concentrations were slightly higher in 2023, the overall geochemical signatures were comparable between years and were consistent with previously reported values [21]. In addition, total organic carbon (TOC) was measured using autoclave-sterilized samples collected in 2022 and was below the detection limit (<3 mg/L).

Next, we tested whether biomass-concentrated incubation reproducibly altered community composition. Filters carrying concentrated biomass collected in each year were incubated in on-site spring water, and both incubations showed similar enrichment trajectories. Strikingly, incubation led to a pronounced shift toward members of the class *Deinococci*, which became the dominant taxon, accounting for 90.5% of the community after 19 days and 83.6% after 95 days (Fig. 1C). In parallel, the relative abundance of Ca. Parcubacteria and *Thermodesulfovibrionia* decreased to 2.8% and 2.7%, respectively.

Downloaded from academic.oup.com/ismecommun/article/6/1/ycag293/8907494 by NATIONAL INSTITUTE FOR MATERIALS SCIENCE user on 18 November 2026

Minor increases in *Actinobacteria* and *Alphaproteobacteria* were also observed after 95 days of incubation. All *Deinococci* sequences enriched during incubation were assigned to the genus *Meiothermus*, and the dominant *Meiothermus* sequence was identical (100% identity across the amplicon region) to a sequence detected in the original environmental samples, indicating enrichment of an indigenous population. Principal coordinate analysis (PCoA) further supported the incubation-driven community shift, with incubated samples clustering distinctly from the original samples and *Deinococci/Meiothermus* contributing most strongly to the observed separation (Supplementary Fig. 1).

Previously characterized cultivated members of the genus *Meiothermus* have been described as obligately aerobic heterotrophs. Therefore, the marked enrichment of *Meiothermus* in incubations designed to minimize oxygen exposure was unexpected. This enrichment may have been supported by residual dissolved oxygen in the spring water, unintentional oxygen entry during incubation, or metabolic capacities that permit survival or growth under oxygen-limited conditions. Regardless of the underlying mechanism, these results show that incubation of concentrated environmental biomass without added organic substrates reproducibly selected for an indigenous *Meiothermus* population that was originally a minor component of the Hakuba–Happo #3 microbial community.

Ultra micro-area filtration enables TEM visualization of incubation-stage-associated cellular structures in extremely low-biomass samples

Direct ultrastructural observation of microorganisms in serpentinization fluids is hampered by extremely low biomass (typically 1–1000 cells mL^{-1}) [23–25] as well as by the limited recovery of intact cells even after conventional filtration (Supplementary Table 3). To overcome these limitations and enable TEM analysis, we developed a UMAF-based concentration method. Briefly, cells resuspended from filters were pre-fixed and subsequently re-concentrated onto a confined micro-area using a 4-mm-diameter suction port, increasing the areal cell density by ∼40-fold (Fig. 2A and B). The UMAF-concentrated spot showed visible brown particulate material (Fig. 2C), consistent with efficient co-concentration of suspended solids from the spring water. Following fixation, embedding, and ultrathin sectioning, cells were readily observed by TEM (Fig. 2D–K), enabling morphological characterization of the enrichment cultures.

In total, 44 TEM fields of view were examined. Of these, 28 fields contained cells with clearly preserved ultrastructural features. In 21 fields, only a single discernible cell was observed, whereas the maximum number of cells observed within a single field was three.

In samples incubated for 6 days, fragmented or apparently lysed cell-like structures were frequently observed (Fig. 2D–G; Supplementary Fig. 2A and B). Rod-shaped cells with thick envelope-like structures were also detected in close proximity to this material (Fig. 2D and E). These observations indicate that cellular debris was abundant during the early stage of incubation and was spatially associated with intact bacterial cells. Although this association alone does not demonstrate uptake or degradation of the debris, it is consistent with the possibility that cell-derived material represented an accessible substrate pool during the enrichment. Sporangium-like structures were also occasionally observed in the 95-day samples (Fig. 2K). Because members of the order *Frankiales* of *Actinomycetota* were detected at low relative abundance in the corresponding community profiles and members of the genus *Frankia* are known to form sporangia [32], these structures may be attributable to *Frankiales*; however, their taxonomic identity could not be determined from morphology alone.

In contrast, in the samples incubated for 95 days, fragmented cell-like structures were no longer observed, and rod-shaped cells with thick-layered structures were the most frequently detected (Fig. 2H–J). Although such cell structures are generally associated with Gram-positive bacteria, members of the phylum *Deinococcota* are also covered by thick cell walls to adapt to extreme environmental stresses [33, 34]. The observed morphologies resembled those reported for *Thermus/Meiothermus* species [35–37]. Because *Meiothermus* accounted for >80% of the 16S rRNA gene community profile at this time point, the predominance of these rod-shaped cells is consistent with, although not definitive evidence for, the abundance of *Meiothermus* in the late-stage enrichment.

Overall, the UMAF method enabled TEM observation of cellular structures in enrichment samples derived from an extremely low-biomass serpentinization fluid. When interpreted together with the 16S rRNA gene amplicon data, the TEM observations revealed an incubation-stage-associated transition from abundant cellular debris and multiple cellular morphologies at the early stage to the predominance of intact, thick-enveloped rod-shaped cells in the *Meiothermus*-dominated late-stage community. This pattern is consistent with, but does not by itself demonstrate, the selective enrichment of microorganisms capable of persisting or growing in the presence of cell-derived organic material.

Genome-resolved metabolic reconstruction of *Meiothermus* suggests the potential for cell-derived substrate heterotrophy under hydrogen-rich conditions

Because *Meiothermus* became enriched even in incubations without exogenously added substrates, a major difference between the incubation and the *in situ* environment was likely the increased availability of biomass resulting from sample concentration and subsequent incubation. We therefore examined whether the *Meiothermus* population enriched during incubation possessed the genetic potential to utilize cell-derived substrates by performing genome-resolved metagenomic analyses.

Using automated binning and refinement (MetaBAT2, MaxBin2.0, and COMEBin), we recovered high-quality *Meiothermus* metagenome-assembled genomes (MAGs) with the completeness of 92.09%–99.8% and contamination of 0.08%–0.16%. The highest quality *Meiothermus* MAG constructed by COMEbin was designated HKB-MT and used for downstream pathway reconstruction.

Because no standardized marker set exists for bacterial cell-derived substrate utilization, we evaluated HKB-MT using a gene-centric framework comprising three functional modules: (i) extracellular depolymerization of cell macromolecules, (ii) uptake of cell-derived substrates, and (iii) intracellular energy conservation and redox balancing compatible with hydrogen-rich conditions.

HKB-MT encoded multiple predicted extracellular serine proteases, consistent with the capacity to hydrolyze proteinaceous biomass (Fig. 3A). This interpretation is supported by previous reports that several *Meiothermus* species produce extracellular serine proteases active under high-temperature and alkaline conditions [38–40]. HKB-MT also encoded a murein DD-endopeptidase (*mepM*), suggesting an

Downloaded from academic.oup.com/ismecommun/article/6/1/ycag293/8907494 by NATIONAL INSTITUTE FOR MATERIALS SCIENCE user on 18 November 2026

additional potential association with processing of peptidoglycan-derived material.

Consistent with the potential uptake of cell-derived solutes, HKB-MT retained an oligopeptide ABC transporter system (*appABCDF*) and a nucleoside transport system (*bmpA–nupABC*) (Fig. 3A), suggesting the capacity to import peptide- and nucleoside-derived substrates released from cellular biomass. A putative glucose/mannose transport system (*msmX–gtsABC*) was also present, indicating a potential route for the uptake of sugar-containing compounds, including those derived from cellular polysaccharides. In contrast, the general L-amino acid transport system (*aapJQMP*) was not detected, suggesting that peptide uptake may be more prominent than uptake of free amino acids in HKB-MT.

Imported peptides could potentially be metabolized through amino acid-to-pyruvate conversion pathways. HKB-MT encoded enzymes associated with the conversion of threonine, serine, glycine, alanine, and cysteine to pyruvate, including *ltaE*, *glyA*, the glycine cleavage system, *tdcB*, *agxT*, and *metC* (Fig. 3A). For nucleoside-derived substrates, HKB-MT encoded genes linking pentose-phosphate metabolism to central carbon metabolism through the non-oxidative pentose phosphate pathway (non-ox-PPP; *deoB*, *rpiA/B*, *rpe*, and *tktA*). Although fructose-bisphosphate aldolase (*fba*) was not detected, enzymes mediating the conversion of glyceraldehyde-3-phosphate to pyruvate were retained. Thus, nucleoside-derived pentose phosphates could potentially enter lower glycolysis via glyceraldehyde-3-phosphate generated through the non-oxidative pentose phosphate pathway. The presence of a putative lactate dehydrogenase (*ldh*) further suggests that pyruvate reduction to lactate may provide a fermentative outlet under oxygen-limited conditions.

HKB-MT encoded metabolic routes for pyruvate utilization under different redox regimes. Genes associated with the tricarboxylic acid cycle (TCA) and respiratory electron transfer were present, consistent with the potential for respiratory metabolism when suitable electron acceptors are available. In addition, HKB-MT encoded pyruvate oxidoreductase (*por*) together with phosphotransacetylase and acetate kinase (*pta* and *ack*), providing a potential route for ATP generation through acetate formation by substrate-level phosphorylation under reducing conditions (Fig. 3A). Despite low nitrate concentrations (Fig. 1B), HKB-MT encoded *narGHI* and *nrfAH* for sequential reduction of nitrate to nitrite and ammonia, indicating potential nitrate respiration when nitrate is available.

HKB-MT also encoded quinone-reactive Ni/Fe-hydrogenase (*hydAB*) and NADH:quinone oxidoreductase (*nqo1*), suggesting the potential to couple H_2 oxidation to NADH generation and respiratory energy conservation when electron acceptors such as O_2 are available. However, because this process does not supply cellular carbon, growth under the incubation conditions likely required organic substrates derived from concentrated cellular biomass.

A potential constraint on this acetate-forming route in hydrogen-rich environments is the reoxidation of reduced ferredoxin generated by Por. In many anaerobic microorganisms, reduced ferredoxin can be reoxidized through hydrogenase-mediated H_2 production [9]; however, net H_2 evolution becomes less favorable as ambient H_2 activity increases. HKB-MT encoded a ferredoxin:$NADP^+$ oxidoreductase (*fprA*), suggesting an alternative route in which reduced ferredoxin could be reoxidized through $NADP^+$ reduction without net H_2 production (Fig. 3B). Consistent with this possibility, thermodynamic calculations indicated that ferredoxin oxidation coupled to $NAD(P)^+$ reduction was energetically favorable under the dissolved H_2 concentration measured at Hakuba–Happo (201 μM), whereas hydrogenase-coupled ferredoxin oxidation through H_2 production was favored under previously reported low-hydrogen conditions (2–60 nM) (Fig. 3C) [41, 42]. This relationship remained robust across the examined range of steady-state-like NADPH/$NADP^+$ ratios (Supplementary Table 4). Furthermore, genes encoding the oxidative pentose phosphate pathway (ox-PPP; *g6pd*, *pgls*, and *pgd*), a common source of NADPH, were not detected, suggesting that FprA may also contribute to NADPH supply in HKB-MT.

Finally, HKB-MT lacked key genes required for the Wood–Ljungdahl pathway (WLP) and the reverse tricarboxylic acid cycle (rTCA), indicating that carbon fixation through these pathways is unlikely. Collectively, these results suggest that the enriched *Meiothermus* population possesses the genetic potential to access protein-, peptide-, and nucleoside-derived components of cellular biomass and to conserve energy from these substrates under reducing, hydrogen-rich conditions.

Fermentative modules occur preferentially in *Meiothermus* MAGs from serpentinization-associated aquifers

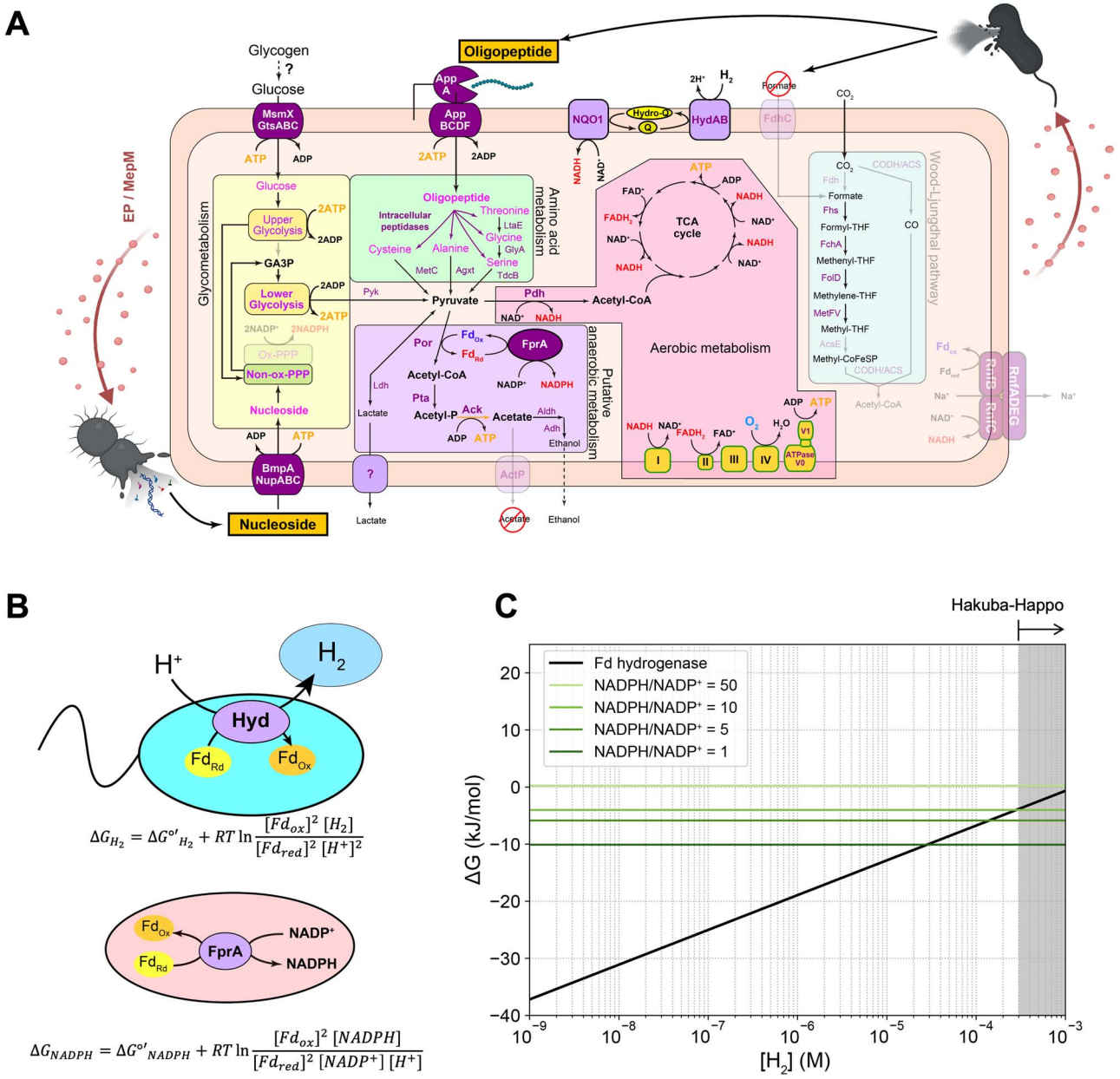
Although the enrichment of *Meiothermus* in our incubations may have been supported by residual oxygen or unintentional oxygen entry, members of this genus have also been repeatedly detected in subsurface serpentinization-associated aquifer systems characterized by highly reducing conditions [21, 43, 44]. In the Samail Ophiolite, phylogenomic and population genomic analyses have identified distinct *Meiothermus* populations associated with shallow and deep aquifer fluids, suggesting lineage diversification within serpentinite-hosted subsurface environments [44]. These observations appear inconsistent with the currently characterized physiology of cultivated *Meiothermus* representatives, which have been described as obligately aerobic heterotrophs. To investigate this point, we performed comparative genomic analyses of publicly available *Meiothermus* isolate genomes and high-quality MAGs (completeness ≥90% and contamination <5%) recovered from diverse environments.

Phylogenomic analysis showed that MAGs from serpentinization-associated aquifers clustered separately from other environmental MAGs and isolate genomes (Fig. 4). Notably, all four serpentinite-aquifer MAGs, including HKB-MT, encoded the Pta–Ack module, consistent with ATP generation via substrate-level phosphorylation, whereas none of the remaining 12 MAGs and genomes encoded this module. Given the presence of Por in HKB-MT, this module provides a potential route for ATP generation through acetate formation from amino acid-derived pyruvate under reducing conditions.

Two *Meiothermus* MAGs recovered from the Sungai Klah hot spring (GCA_025056915 and GCA_025060375) encoded lactate dehydrogenase, suggesting a potential route for pyruvate reduction to lactate. Sungai Klah is characterized by substantial plant litter inputs and relatively high organic matter availability [46], conditions that may support carbohydrate-associated heterotrophic metabolism. However, because oxygen availability at the specific sampling positions represented by these MAGs has not been directly established, the presence of lactate dehydrogenase alone cannot be taken as evidence of anaerobic growth *in situ*.

In contrast, none of the aerobically isolated *Meiothermus* genomes encoded acetate, lactate, and alcohol fermentative pathway modules from pyruvate, consistent with their obligate aerobic lifestyle (Fig. 4).

Downloaded from academic.oup.com/ismecommun/article/6/1/ycag293/8907494 by NATIONAL INSTITUTE FOR MATERIALS SCIENCE user on 18 November 2026



$$\Delta G_{H_2} = \Delta G^{o\prime}{}_{H_2} + RT \ln \frac{[Fd_{ox}]^2\,[H_2]}{[Fd_{red}]^2\,[H^+]^2}$$

$$\Delta G_{NADPH} = \Delta G^{o\prime}{}_{NADPH} + RT \ln \frac{[Fd_{ox}]^2\,[NADPH]}{[Fd_{red}]^2\,[NADP^+]\,[H^+]}$$

Figure 3 Genome-informed model of candidate cell-derived substrate utilization and hydrogen-independent ferredoxin reoxidation in the HKB-MT *Meiothermus* MAG. (A) Predicted pathways for utilization of cell-derived substrates. Extracellular proteases and cell-wall–targeting peptidase (MepM) are predicted to release soluble substrates from cell-derived materials, which are imported via an oligopeptide transporter (AppABCDF), a nucleoside transporter (BmpA–NupABC) and a sugar transporter (MsmX–GtsABC). Imported carbon is predicted to converge on pyruvate and acetate formation via Por–Pta–Ack, potentially enabling ATP generation by substrate-level phosphorylation. Genes detected in HKB-MT are shown in purple; genes not detected are shown in gray (semi-transparent). Detailed map of glycometabolism and abbreviations are provided in Supplementary Fig. 5 and Supplementary Table 6. A schematic illustration of ruptured microbial cells was created using https://BioRender.com. (B) Conceptual comparison of ferredoxin reoxidation routes coupled to pyruvate oxidation: proton reduction to H_2 via ferredoxin-dependent hydrogenase versus $NADP^+$ reduction via ferredoxin–$NADP^+$ reductase (FprA), potentially enabling redox balancing without net H_2 evolution. (C) Calculated ΔG change for ferredoxin oxidation via hydrogenase (black) and via Fd:$NADP^+$ oxidoreductase (green) as a function of dissolved H_2 concentration. For the Fd:$NADP^+$ oxidoreductase, the NADPH/$NADP^+$ ratio was varied (1, 5, 10, and 50), with colors ranging from dark green to light green accordingly. The gray band indicates dissolved H_2 concentrations at or above the value measured at Hakuba–Happo (201 μM). The redox ratio of intracellular ferredoxin was fixed at unity (i.e. $Fd_{red}/Fd_{ox} = 1$). Negative ΔG values indicate thermodynamic favorability.

Two MAGs recovered from the Katase hot spring (GCA_026004055 and GCA_026004115) also lacked these fermentative pathways; dissolved oxygen concentrations of 3.85 mg L^{-1} have been reported at this site [47], consistent with the feasibility of aerobic respiration.

Collectively, these comparative genomic analyses show that pyruvate-linked fermentative modules are not uniformly distributed across the genus *Meiothermus*. In particular, the Pta–Ack acetate-forming module was uniquely detected, among the genomes

Downloaded from academic.oup.com/ismecommun/article/6/1/ycag293/8907494 by NATIONAL INSTITUTE FOR MATERIALS SCIENCE user on 18 November 2026

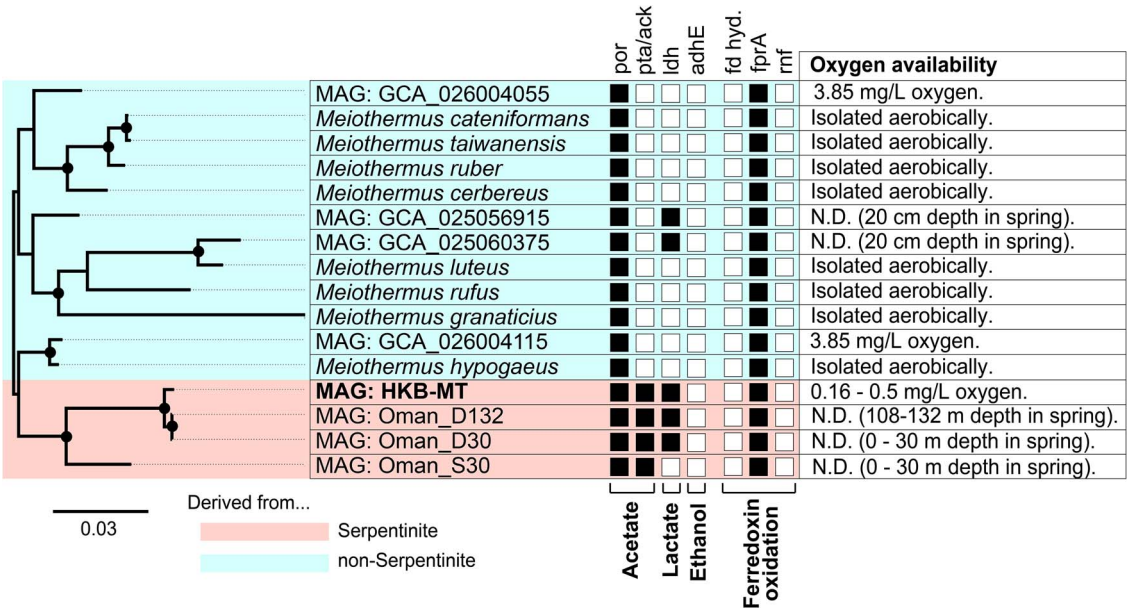


Figure 4 Phylogenomic distribution of pyruvate-derived fermentative modules in serpentinite- and non-serpentinite-derived *Meiothermus*. Phylogenomic tree constructed from high-quality *Meiothermus* isolate genomes and MAGs ($n = 16$; completeness ≥90% and contamination <5%) recovered from serpentinite and non-serpentinite environments. The matrix indicates the presence (filled squares) or absence (empty squares) of fermentative modules derived from pyruvate (acetate, lactate, and ethanol pathways) and genes involved in ferredoxin oxidation. Ferredoxin hydrogenase (fd hyd.) genes were investigated using HydDB [45]. Branch support values ≥90% ultrafast bootstrap and ≥80% SH-aLRT are indicated by black circles. GenBank accession numbers, sampling site information, and references used in this figure are listed in Supplementary Table 7. N.D., not determined.

examined here, in MAGs recovered from serpentinization-associated aquifers. These findings do not demonstrate anaerobic growth of *Meiothermus in situ* or in our incubations; however, they indicate that uncultivated serpentinite-associated populations possess metabolic capacities not observed in the cultivated aerobic representatives analyzed here. Together with the metabolic reconstruction of HKB-MT, this distribution supports the hypothesis that acetate-forming metabolism may contribute to the persistence or enrichment of specific *Meiothermus* populations under hydrogen-rich, reducing conditions.

Distribution of candidate cell-derived substrate heterotrophy modules across serpentinite-hosted microbiomes

To examine whether the metabolic features identified in HKB-MT are present in other serpentinite-hosted microbial communities, we screened a total of 331 MAGs derived from 15 serpentinite-hosted metagenomic datasets spanning six systems [Hakuba–Happo #3; Oman Samail Ophiolite (BA1A); The Cedars (GPS1, BS5); CROMO (CSWold, CSW1.1, QV1.1); Voltri Massif (BR2-spring, GOR34-spring3); and Lost City; Supplementary Table 1; Supplementary Data 1]. We curated a KEGG Orthology (KO)-based marker set representing (i) extracellular depolymerization, (ii) uptake of cell-derived substrates, and (iii) intracellular catabolism of peptide- and/or nucleoside-derived carbon into central metabolism (Supplementary Data 2).

Focusing on high-quality MAGs (completeness ≥90% and contamination <5%), we identified 18 genomes that encoded gene complements consistent with intracellular utilization of oligopeptide- and/or nucleoside-derived substrates together with hydrogen-independent ferredoxin oxidation modules (Fig. 5A). These MAGs spanned phylogenetically diverse lineages including *Meiothermus*, *Bacillota* class UBA994, *Dethiobacteraceae, Silanimonas, Serpentinimonas, Endomicrobiia*, and *Bacteroidales*, and were recovered from all systems examined except Lost City (Fig. 5A).

Across these 18 MAGs, modules associated with protein-derived substrates were more prevalent than those for nucleoside uptake. More than half of the MAGs encoded extracellular serine proteases, and oligopeptide transport systems were detected in a larger fraction of genomes than nucleoside transport systems (Fig. 5A). This distribution is consistent with protein representing a major component of cell-derived substrate.

Notably, only *Meiothermus* MAGs and a subset of *Bacillota* class UBA994 MAGs combined extracellular proteolysis with uptake capacity for both oligopeptides (AppABCDF) and nucleosides (BmpA–NupABC). These lineages therefore possess comparatively broad genetic capacities for accessing multiple fractions of cell-derived organic matter. UBA994 MAGs generally encoded a limited set of enzymes for pyruvate formation restricted to threonine, glycine, and serine catabolism. Moreover, UBA994 MAGs were recovered from lower-temperature serpentinite-hosted sites in which *Meiothermus* was not detected, suggesting that this lineage may represent an additional candidate contributor to cell-derived substrate utilization across serpentinite environments. In contrast, *Endomicrobiia* and *Serpentinimonas* encoded complete or partial AppABCDF gene sets together with conserved intracellular peptide-catabolic modules, but generally lacked nucleoside-transport modules, suggesting a more peptide-focused metabolic potential.

We next examined whether these candidate necromass-derived substrate utilizers encoded hydrogen-independent routes for reoxidation of reduced ferredoxin, because HKB-MT contained the FprA as a potential alternative to hydrogenase-mediated H_2 production. The FprA identified in HKB-MT was restricted to the genus *Meiothermus*, whereas all other putative cell-derived substrate utilizers encoded the

Downloaded from academic.oup.com/ismecommun/article/6/1/ycag293/8907494 by NATIONAL INSTITUTE FOR MATERIALS SCIENCE user on 18 November 2026

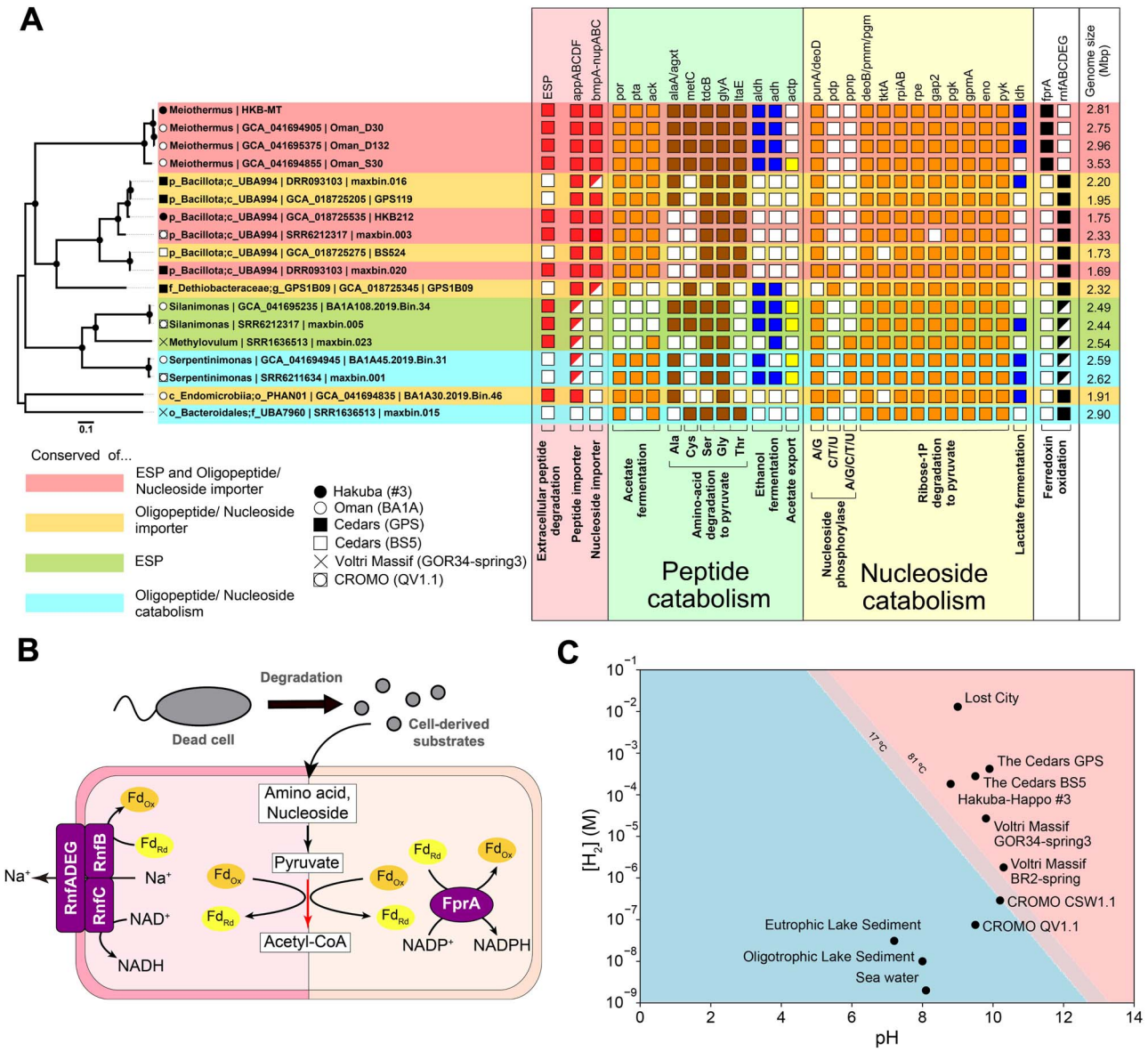


Figure 5 Phylogenetic distribution of candidate cell-derived substrate catabolism and hydrogen-independent ferredoxin reoxidation across serpentinite-hosted microbiomes. (A) Phylogenomic tree of high-quality MAGs ($n = 18$; completeness ≥90% and contamination <5%) identified from a screen of 331 MAGs derived from 15 serpentinite-hosted metagenomic datasets (Supplementary Data 1) using a curated KO-based marker set (Supplementary Data 2). Symbols denote the site of origin. The matrix summarizes the presence (filled squares), partial presence (half-filled squares; subset of genes within a multi-gene set), or absence (empty squares) of modules grouped by function: extracellular depolymerization (extracellular serine protease, ESP), substrate uptake (AppABCDF oligopeptide transporter; BmpA–NupABC nucleoside transporter), intracellular peptide and nucleoside catabolism into central metabolism, and hydrogen independent ferredoxin oxidation. Branches supported by ≥90% ultrafast bootstrap and ≥80% SH-aLRT are marked with black circles. Genome size (Mbp) is shown at right. Abbreviations are provided in Supplementary Table 6. The matrix reflects gene presence/absence and does not by itself demonstrate *in situ* activity. (B) Conceptual model of hydrogen-independent ferredoxin reoxidation modules identified among candidate MAGs with genomic potential for cell-derived substrate utilization. The Rnf complex couples ferredoxin oxidation to NAD^+ reduction and conserves energy as a Na^+ motive force, whereas FprA enables ferredoxin oxidation via $NADP^+$ reduction to NADPH. (C) Thermodynamic phase space for ferredoxin reoxidation pathways as a function of pH and dissolved hydrogen concentration. Background shading indicates conditions favoring $NAD(P)^+$-linked ferredoxin oxidation (pale red) versus hydrogenase-catalyzed H_2 evolution (pale blue); points indicate pH and $[H_2]$ values for serpentinite-hosted systems and reference environments (Supplementary Table 3). For serpentinite-hosted systems, plotted pH values represent assumed intracellular pH, set two units below the corresponding environmental pH [23]. The redox ratios of intracellular compounds were fixed at unity (i.e. $NAD(P)H/NAD(P)^+ = 1$, $Fd_{red}/Fd_{ox} = 1$).

Na^+-translocating ferredoxin:NAD^+ oxidoreductase (Rnf; rnfABCDEG) complex (Fig. 5A and B). Thus, although the enzyme systems differed among lineages, the candidate populations examined here possessed $NAD(P)^+$-linked routes for ferredoxin reoxidation without net H_2 production. None of the 18 MAGs encoded complete WLP or rTCA gene sets, supporting their interpretation as heterotrophic populations rather than organisms fixing carbon through these pathways (Supplementary Fig. 3).

Thermodynamic analysis further showed that, except at the two lowest-H_2 CROMO sites (CSW1.1 and QV1.1), the reported

Downloaded from academic.oup.com/ismecommun/article/6/1/ycag293/8907494 by NATIONAL INSTITUTE FOR MATERIALS SCIENCE user on 18 November 2026

pH and dissolved H_2 conditions of the surveyed systems fell within a range in which NAD(P)$^+$-linked ferredoxin oxidation was favored relative to hydrogenase-mediated H_2 production (Fig. 5C; Supplementary Fig. 4; Supplementary Table 3). Although these calculations do not demonstrate pathway activity *in situ*, they indicate that hydrogen-independent ferredoxin reoxidation is thermodynamically compatible with the conditions of most surveyed serpentinite-hosted systems.

Collectively, these results suggest that diverse heterotrophic populations in serpentinite-hosted environments possess genetic capacities to utilize peptide- and/or nucleoside-derived components of cellular biomass. The recurrent association of these capacities with either FprA or Rnf further suggests that hydrogen-independent ferredoxin reoxidation may support cell-derived substrate metabolism under hydrogen-rich conditions, with *Meiothermus* representing a lineage employing a distinct putative FprA-dependent strategy.

Discussion

Serpentinite-hosted ecosystems are widely viewed as paradigmatic lithoautotrophic communities fueled by abundant H_2 and limited availability of terminal electron acceptors [23]. Our study extends this framework by identifying microbial populations with the genetic potential to utilize cell-derived organic matter in serpentinite-hosted environments. In biomass-concentrated incubations without added organic substrates, an indigenous *Meiothermus* population, initially representing only a minor component of the Hakuba–Happo #3 community, became strongly enriched. Although the contribution of residual or inadvertently introduced O_2 cannot be excluded, the observed community shift, together with TEM detection of cellular debris during early incubation and the metabolic reconstruction of HKB-MT, is consistent with selection for a *Meiothermus* population capable of accessing cell-derived substrates. Importantly, genome-resolved and thermodynamic analyses further suggest that serpentinite-associated *Meiothermus* populations possess metabolic capacities that could support heterotrophic energy conservation under hydrogen-rich, reducing conditions. This provides a possible explanation for the repeated detection of *Meiothermus* in serpentinization-associated aquifers despite the aerobic phenotypes reported for cultivated representatives of this genus. Beyond *Meiothermus*, comparative analyses across multiple serpentinite-hosted metagenomic datasets identified phylogenetically diverse populations encoding candidate modules for the uptake and metabolism of cell-derived substrates. Although our analyses do not directly demonstrate necromass recycling *in situ*, they identify a previously underappreciated set of candidate heterotrophs that may contribute to carbon turnover in serpentinite-hosted microbial communities.

The genomic characteristics of serpentinite-associated *Meiothermus* further suggest that uncultivated members of this lineage may differ metabolically from cultivated aerobic representatives. Specifically, all serpentinite-derived *Meiothermus* MAGs examined here encoded the Pta–Ack acetate-forming module, whereas this module was absent from the other *Meiothermus* genomes included in our comparison. The coexistence of respiratory and fermentative modules supports a scenario in which these lineages adapted to electron-acceptor-limited anoxic environments through the incorporation of fermentative metabolism. Under hydrogen-rich conditions, conventional anaerobic amino acid catabolism coupled to disposal of reduced ferredoxin through H_2 production is expected to become thermodynamically constrained [11–13]. In contrast, the NAD(P)$^+$-linked ferredoxin-reoxidation routes identified here (FprA and/or Rnf) provide potential hydrogen-independent alternatives for redox balancing (Figs 3C and 5C).

Based on our thermodynamic calculations, we screened for putative enzymes enabling anaerobic amino acid metabolism under H_2-rich conditions and identified NAD(P)$^+$-linked ferredoxin oxidoreductases as candidate systems. Candidate necromass-metabolizing bacteria encoding these systems were distributed across phylogenetically diverse lineages and geographically distinct serpentinite-hosted environments. Among these lineages, *Bacillota* class UBA994 was detected across multiple serpentinite-hosted sites spanning low-temperature to mesophilic conditions. UBA994 is currently recognized as an uncultivated lineage affiliated with *Clostridia*, and genome-based studies have suggested the potential for spore formation [23,48]. Our results provide new ecological context by indicating that UBA994 genomes can encode combinations of extracellular proteolysis, peptide uptake, and peptide catabolism consistent with cell-derived substrate utilization. Given its phylogenetic proximity to *Clostridia*, it will be of particular interest to resolve whether this lineage retains potentially ancient redox-balancing strategies (e.g. Rnf-based energy conservation) that may be advantageous in hydrogen-rich environments. However, the observation that genes associated with fermentative pathways for NADH reoxidation from pyruvate (*aldh*, *adh*, and *ldh*) were rarely detected within the UBA994 clade (Fig. 5A) raises questions regarding how this lineage maintains intracellular redox balance. In our additional survey, several UBA994 MAGs lacked genes associated with fumarate, nitrate, oxygen, or sulfate respiration, leaving the mechanism of NADH reoxidation unresolved (data not shown). Previous studies have reported that some members of UBA994 encode an H_2-dependent glycine reduction pathway capable of generating ATP [23]. If so, energy conservation in this lineage may rely primarily on this metabolic route, whereas peptides and nucleosides derived from necromass may mainly support biosynthetic demands rather than serving as major energy substrates. These interpretations remain provisional and motivate targeted cultivation efforts and functional assays to validate substrate preferences and energy-conservation mechanisms.

This perspective complements, rather than replaces, the prevailing emphasis on lithoautotrophic acetogenesis in serpentinite research. The WLP is widely regarded as one of the most primordial carbon-fixation pathways, and acetogenic energy conservation has therefore occupied a central role in models of early life evolution [49–52]. Accordingly, serpentinite-hosted systems, frequently discussed as geochemical analogues of early Earth settings, have been investigated primarily through the lens of hydrogen-oxidizing lithoautotrophic acetogens [20,22,23,53]. However, the extent to which serpentinite-associated acetogens are obligate autotrophs remains unresolved, and many characterized acetogens exhibited mixotrophy, utilizing organic substrates when available. A key constraint on strict autotrophy via the WLP is reliance on metabolically expensive cofactors such as corrinoids (vitamin B_{12}) [54,55]. Fewer than ~40% of microbial taxa are estimated to encode complete *de novo* cobalamin biosynthesis pathways [56,57], implying that corrinoid salvage and exchange are likely widespread. In line with this interpretation, our Prokka- and KofamScan-based annotations indicate that serpentinite-hosted MAGs encoding acetogenic carbon-fixation pathways commonly retain vitamin B_{12} transporter components (e.g. *btuB* and/or *btuD*), and, in some cases, also encode transporters for other microbially

Downloaded from academic.oup.com/ismecommun/article/6/1/ycag293/8907494 by NATIONAL INSTITUTE FOR MATERIALS SCIENCE user on 18 November 2026

derived compounds (Supplementary Table 5). These patterns are consistent with the possibility of metabolic interdependence within serpentinite communities and highlight that community-derived organic inputs including vitamins and necromass-derived metabolites may contribute to sustaining lithoautotrophic processes *in situ*.

These findings also help reconcile contradictory observations in serpentinite systems: low cell abundances in bulk fluids versus long-term persistence of diverse microbial communities despite limited primary productivity, and, in some cases, high localized activity on solid surfaces. Surface-associated microhabitats (e.g. mineral pores and fracture walls) can reach cell densities orders of magnitude higher than those in surrounding fluids, creating conditions under which necromass is both continuously generated and readily encountered. Under crowded, carbon-limited conditions, preferential assimilation of cell-derived substrates has been reported in other microbial systems [27–29], consistent with necromass becoming a predictable resource in dense microhabitats. In such settings, cell-derived substrate metabolism may provide not only carbon and energy but also essential biomolecules (e.g. nucleosides and cofactors) that are costly to synthesize *de novo*, raising the possibility that such processes contribute to community stability under chronic energy limitation.

We note that our comparative screen did not identify high-quality MAGs meeting our cell-derived substrate utilization criteria from the Lost City datasets. This absence may reflect genuine ecological differences (e.g. site-specific constraints on organic substrate availability or biofilm structure) but may also result from dataset-specific factors such as sampling strategy, size fractionation, sequencing depth, assembly and binning recovery, or our conservative completeness and contamination thresholds. Indeed, many MAGs reported from the Lost City hydrothermal field have been classified as medium or lower quality [58]. Expanded sampling and standardized, cross-site metagenomic processing will help determine whether cell-derived substrate-based heterotrophy is genuinely reduced at Lost City or simply undetected.

Thermodynamic comparisons inevitably depend on intracellular redox ratios, which remain poorly constrained for uncultivated serpentinite microorganisms. Previous studies have shown that the $NADH/NAD^+$ ratio is generally maintained at low levels under steady-state conditions, whereas the $NADPH/NADP^+$ ratio is typically closer to unity and becomes much higher mainly during rapid exponential growth (Supplementary Table 4). Because serpentinite-hosted systems are strongly energy-limited, steady-state-like redox conditions are more plausible than exponential-growth-like conditions. Under this assumption, our sensitivity analysis showed that $NADP^+$-linked ferredoxin oxidation remained more favorable than ferredoxin-dependent hydrogenase up to a $NADPH/NADP^+$ ratio of ~10 (Fig. 3C). By contrast, quantitative constraints on the ferredoxin redox state are scarce; we therefore fixed Fd_{red}/Fd_{ox} at 1 as a simplifying assumption and interpret these calculations primarily as a comparison of relative thermodynamic favorability rather than an exact prediction of intracellular ΔG values. Notably, because both competing pathways involve the same ferredoxin redox couple, variation in Fd_{red}/Fd_{ox} should affect the absolute ΔG values of both reactions similarly and is therefore unlikely to substantially alter the crossover between them.

Finally, we demonstrate that the UMAF-based concentration approach enables TEM imaging from extremely low-biomass serpentinite-hosted samples. While cell numbers remain limiting, concentrating large volumes onto a micro-area substantially improves the feasibility of ultrastructural analyses. This methodological advance may be particularly useful for investigating lineages such as Ca. Parcubacteria (formerly referred to as candidate division OD1), which often dominate serpentinite-hosted communities yet lack genes considered essential for independent survival, consistent with endo- or ectosymbiotic lifestyles [59]. UMAF-enabled imaging could help identify potential symbiotic partners and characterize physical interaction modes *in situ*.

In summary, our results suggest that heterotrophic populations with genetic potential to access cell-derived substrates may persist in hydrogen-rich serpentinite-hosted ecosystems through hydrogen-independent ferredoxin reoxidation. This possibility broadens the prevailing lithoautotrophy-centered view of these environments and raises the possibility that cell-derived substrate metabolism may contribute to carbon turnover in serpentinite-hosted microbial communities, although its occurrence *in situ* remains to be demonstrated. Future oxygen-controlled cultivation, isotope-labeled substrate experiments, and transcriptomic or proteomic analyses will be required to test whether these candidate pathways are active under environmentally relevant conditions.

Acknowledgements

The authors gratefully acknowledge Happo-one Development Co., Ltd for their permission and kind cooperation in facilitating the field studies at Hakuba Happo hot springs.

Author contributions

S.I. and A.O. designed the research; S.I., H.H., R.N., H.T., and A.O. performed the sampling; S.I. performed the experiments and metagenomic analysis; S.I. and H.H. performed microbiome analysis; H.T. and A.O. supervised the study; S.I. and A.O. wrote the final version of the manuscript. All authors read and agreed to the submitted version of the manuscript.

Supplementary material

Supplementary material is available at *ISME Communications* online.

Conflicts of interest

None declared.

Funding

This work was financially supported by a Grant-in-Aid for Research from the Japan Society for Promotion of Science (JSPS) KAKENHI (Grant No. JP22KK0242), and Grant-in-Aid for JSPS Fellows (Grant No. JP24KJ0484). This work was also supported by the Japan Agency for Medical Research and Development (21ae0121044h0001 to A.O) and Japan Science and Technology Agency (JST), the establishment of university fellowships towards the creation of science technology innovation (Grant No. JPMJSP2124), and by the JAEA Nuclear Energy S&T and Human Resource Development Project through concentrating wisdom (Grant No. PJA24P24021180).

Data availability

The 16S rRNA amplicon sequences (DRR749208 – DRR749209 under DRA022538 and DRR898348-DRR898349), and MAG data of

Downloaded from academic.oup.com/ismecommun/article/6/1/ycag293/8907494 by NATIONAL INSTITUTE FOR MATERIALS SCIENCE user on 18 November 2026

HKB-MT (BioSample Accession: SAMD01687034) were deposited into DDBJ under BioProject accession no. PRJDB37557 and PRJDB37697.

Declaration of AI use

The authors (S.I. and A.O.) used ChatGPT (GPT-5.2) for English-language proofreading of this manuscript. After using this tool, the authors carefully reviewed and edited the content.

References

1. Camenzind T, Mason-Jones K, Mansour I, *et al.* Formation of necromass-derived soil organic carbon determined by microbial death pathways. *Nat Geosci* 2023;**16**:115–22. https://doi.org/10.1038/s41561-022-01100-3
2. Finley BK, Enalls BC, de Raad M, *et al.* Unraveling the influence of microbial necromass on subsurface microbiomes: metabolite utilization and community dynamics. *ISME Commun* 2025;**5**:ycaf006. https://doi.org/10.1093/ismeco/ycaf006
3. Wang B, An S, Liang C, *et al.* Microbial necromass as the source of soil organic carbon in global ecosystems. *Soil Biol Biochem* 2021;**162**:108422. https://doi.org/10.1016/j.soilbio.2021.108422
4. Lomstein BA, Langerhuus AT, D'Hondt S, *et al.* Endospore abundance, microbial growth and necromass turnover in deep subseafloor sediment. *Nature.* 2012;**484**:101–4. https://doi.org/10.1038/nature10905
5. Geesink P, Taubert M, Jehmlich N, *et al.* Bacterial necromass is rapidly metabolized by heterotrophic bacteria and supports multiple trophic levels of the groundwater microbiome. *Microbiol Spectr* 2022;**10**:e00437–22. https://doi.org/10.1128/spectrum.00437-22
6. Shoemaker WR, Jones SE, Muscarella ME, *et al.* Microbial population dynamics and evolutionary outcomes under extreme energy limitation. *Proc Natl Acad Sci* 2021;**118**:e2101691118. https://doi.org/10.1073/pnas.2101691118
7. Feijo Delgado F, Cermak N, Hecht VC, *et al.* Intracellular water exchange for measuring the dry mass, water mass and changes in chemical composition of living cells. *PLoS One* 2013;**8**:e67590. https://doi.org/10.1371/journal.pone.0067590
8. Stouthamer AH. A theoretical study on the amount of atp required for synthesis of microbial cell material. *Antonie Van Leeuwenhoek* 1973;**39**:545–65. https://doi.org/10.1007/BF02578899
9. Canfield DE, Kristensen E, Thamdrup B. Thermodynamics and microbial metabolism. *Adv Mar Biol* 2005;**48**:65–94. https://doi.org/10.1016/S0065-2881(05)48003-7
10. Barker HA. Amino acid degradation by anaerobic bacteria. *Annu Rev Biochem* 1981;**50**:23–40. https://doi.org/10.1146/annurev.bi.50.070181.000323
11. Schink B. Energetics of syntrophic cooperation in methanogenic degradation. *Microbiol Mol Biol Rev* 1997;**61**:262–80. https://doi.org/10.1128/mmbr.61.2.262-280.1997
12. Winter J, Schindler F, Wildenauer FX. Fermentation of alanine and glycine by pure and syntrophic cultures of clostridium sporogenes. *FEMS Microbiol Ecol* 1987;**3**:153–61. https://doi.org/10.1111/j.1574-6968.1987.tb02351.x
13. Adams CJ, Redmond MC, Valentine DL. Pure-culture growth of fermentative bacteria, facilitated by H_2 removal: bioenergetics and H_2 production. *Appl Environ Microbiol* 2006;**72**:1079–85. https://doi.org/10.1128/AEM.72.2.1079-1085.2006
14. Smith NJP, Shepherd TJ, Styles MT, *et al.* Hydrogen exploration: a review of global hydrogen accumulations and implications for prospective areas in NW Europe. *Geological Society, London, Petroleum Geology Conference Series* 2005;**6**:349–58. https://doi.org/10.1144/0060349
15. Piché-Choquette S, Constant P. Molecular hydrogen, a neglected key driver of soil biogeochemical processes. *Appl Environ Microbiol* 2019;**85**:e02418–18. https://doi.org/10.1128/AEM.02418-18
16. Worman SL. *Global Rates of Free Hydrogen (H_2) Production by Serpentinization and Other Abiogenic Processes within Young Ocean Crust*. Doctoral dissertation, Durham, NC: Duke University, 2015.
17. Holm NG, Oze C, Mousis O, *et al.* Serpentinization and the formation of H_2 and CH_4 on celestial bodies (planets, moons, comets). *Astrobiology* 2015;**15**:587–600. https://doi.org/10.1089/ast.2014.1188
18. Martin W, Baross J, Kelley D, *et al.* Hydrothermal vents and the origin of life. *Nat Rev Microbiol* 2008;**6**:805–14. https://doi.org/10.1038/nrmicro1991
19. Suda K, Ueno Y, Yoshizaki M, *et al.* Origin of methane in serpentinite-hosted hydrothermal systems: the CH_4–H_2–H_2O hydrogen isotope systematics of the Hakuba Happo hot spring. *Earth Planet Sci Lett* 2014;**386**:112–25. https://doi.org/10.1016/j.epsl.2013.11.001
20. Suzuki S, Nealson KH, Ishii S. Genomic and in-situ transcriptomic characterization of the candidate phylum NPL-UPL2 from highly alkaline highly reducing serpentinized groundwater. *Front Microbiol* 2018;**9**:3141. https://doi.org/10.3389/fmicb.2018.03141
21. Merino N, Kawai M, Boyd ES, *et al.* Single-cell genomics of novel actinobacteria with the Wood-Ljungdahl pathway discovered in a serpentinizing system. *Front Microbiol* 2020;**11**:1031. https://doi.org/10.3389/fmicb.2020.01031
22. Suzuki S, Ishii S, Chadwick GL, *et al.* A non-methanogenic archaeon within the order *Methanocellales*. *Nat Commun* 2024;**15**:4858. https://doi.org/10.1038/s41467-024-48185-5
23. Nobu MK, Nakai R, Tamazawa S, *et al.* Unique H_2-utilizing lithotrophy in serpentinite-hosted systems. *ISME J* 2023;**17**:95–104. https://doi.org/10.1038/s41396-022-01197-9
24. Suzuki S, Ishii S, Wu A, *et al.* Microbial diversity in The Cedars, an ultrabasic, ultrareducing, and low salinity serpentinizing ecosystem. *Proc Natl Acad Sci* 2013;**110**:15336–41. https://doi.org/10.1073/pnas.1302426110
25. Colman DR, Templeton AS, Spear JR, *et al.* Microbial ecology of serpentinite-hosted ecosystems. *ISME J* 2025;**19**:wraf029. https://doi.org/10.1093/ismejo/wraf029
26. Morrill PL, Kuenen JG, Johnson OJ, *et al.* Geochemistry and geobiology of a present-day serpentinization site in California: The Cedars. *Geochim Cosmochim Acta* 2013;**109**:222–40. https://doi.org/10.1016/j.gca.2013.01.043
27. Takano S, Pawlowska BJ, Gudelj I, *et al.* Density-dependent recycling promotes the long-term survival of bacterial populations during periods of starvation. *mBio.* 2017;**8**:e02336–16. https://doi.org/10.1128/mBio.02336-16
28. Zinser ER, Kolter R. Mutations enhancing amino acid catabolism confer a growth advantage in stationary phase. *J Bacteriol* 1999;**181**:5800–7. https://doi.org/10.1128/jb.181.18.5800-5807.1999
29. Zinser ER, Kolter R. Prolonged stationary-phase incubation selects for lrp mutations in *Escherichia coli* K-12. *J Bacteriol* 2000;**182**:4361–5. https://doi.org/10.1128/jb.182.15.4361-4365.2000
30. Capella-Gutierrez S, Silla-Martinez JM, Gabaldon T. TrimAl: a tool for automated alignment trimming in large-scale phylogenetic analyses. *Bioinformatics.* 2009;**25**:1972–3. https://doi.org/10.1093/bioinformatics/btp348
31. Minh BQ, Schmidt HA, Chernomor O, *et al.* IQ-TREE 2: new models and efficient methods for phylogenetic inference in the genomic era. *Mol Biol Evol* 2020;**37**:1530–4. https://doi.org/10.1093/molbev/msaa015

Downloaded from academic.oup.com/ismecommun/article/6/1/ycag293/8907494 by NATIONAL INSTITUTE FOR MATERIALS SCIENCE user on 18 November 2026

32. Nouioui I, Ghodhbane-Gtari F, Jando M, *et al. Frankia colletiae* sp. nov., a nitrogen-fixing actinobacterium isolated from *Colletia cruciata*. *Int J Syst Evol Microbiol* 2023;**73**:005656. https://doi.org/10.1099/ijsem.0.005656
33. von Kugelgen A, van Dorst S, Alva V, *et al.* A multidomain connector links the outer membrane and cell wall in phylogenetically deep-branching bacteria. *Proc Natl Acad Sci* 2022;**119**:e2203156119. https://doi.org/10.1073/pnas.2203156119
34. Cava F, de Pedro MA, Schwarz H, *et al.* Binding to pyruvylated compounds as an ancestral mechanism to anchor the outer envelope in primitive bacteria. *Mol Microbiol* 2004;**52**:677–90. https://doi.org/10.1111/j.1365-2958.2004.04011.x
35. Fernández-Herrero LA, Olabarria G, Castón JR, *et al.* Horizontal transference of S-layer genes within *Thermus thermophilus*. *J Bacteriol* 1995;**177**:5460–6. https://doi.org/10.1128/jb.177.19.5460-5466.1995
36. Chen MY, Lin GH, Lin YT, *et al. Meiothermus taiwanensis* sp. nov., a novel filamentous, thermophilic species isolated in Taiwan. *Int J Syst Evol Microbiol* 2002;**52**:1647–54. https://doi.org/10.1099/ijs.0.02189-0
37. Yamaoka A, Kataoka M, Kawasaki K, *et al. Meiothermus ruber* H328 enhances the production of membrane vesicles for feather degradation. *Biosci Biotechnol Biochem* 2014;**78**:1623–5. https://doi.org/10.1080/09168451.2014.918488
38. Wu WL, Chen MY, Tu IF, *et al.* The discovery of novel heat-stable keratinases from *Meiothermus taiwanensis* WR-220 and other extremophiles. *Sci Rep* 2017;**7**:4658. https://doi.org/10.1038/s41598-017-04723-4
39. Lien YC, Lai SJ, Lin CY, *et al.* High-efficiency decomposition of eggshell membrane by a keratinase from *Meiothermus taiwanensis*. *Sci Rep* 2022;**12**:14684. https://doi.org/10.1038/s41598-022-18474-4
40. Yamamoto F, Morisaka H, Ueda M, *et al.* Molecular characterization of a prolyl endopeptidase from a feather-degrading thermophile *Meiothermus ruber* H328. *J Biochem* 2020;**168**:499–508. https://doi.org/10.1093/jb/mvaa069
41. Krämer H, Conrad R. Measurement of dissolved H_2 concentrations in methanogenic environments with a gas diffusion probe. *FEMS Microbiol Ecol* 1993;**12**:149–58. https://doi.org/10.1111/j.1574-6941.1993.tb00027.x
42. Lappan R, Shelley G, Islam ZF, *et al.* Molecular hydrogen in seawater supports growth of diverse marine bacteria. *Nat Microbiol* 2023;**8**:581–95. https://doi.org/10.1038/s41564-023-01322-0
43. Woycheese KM, Meyer-Dombard DAR, Cardace D, *et al.* Out of the dark: transitional subsurface-to-surface microbial diversity in a terrestrial serpentinizing seep (Manleluag, Pangasinan, the Philippines). *Front Microbiol* 2015;**6**:44. https://doi.org/10.3389/fmicb.2015.00044
44. Munro-Ehrlich M, Nothaft DB, Fones EM, *et al.* Parapatric speciation of *Meiothermus* in serpentinite-hosted aquifers in Oman. *Front Microbiol* 2023;**14**:1138656. https://doi.org/10.3389/fmicb.2023.1138656
45. Sondergaard D, Pedersen CNS, Greening C. HydDB: a web tool for hydrogenase classification and analysis. *Sci Rep* 2016;**6**:34212. https://doi.org/10.1038/srep34212
46. Liew KJ, Liang CH, Lau YT, *et al.* Thermophiles and carbohydrate-active enzymes (CAZymes) in biofilm microbial consortia that decompose lignocellulosic plant litters at high temperatures. *Sci Rep* 2022;**12**:2850. https://doi.org/10.1038/s41598-022-06943-9
47. Kato S, Masuda S, Shibata A, *et al.* Insights into ecological roles of uncultivated bacteria in Katase hot spring sediment from long-read metagenomics. *Front Microbiol* 2022;**13**:1045931. https://doi.org/10.3389/fmicb.2022.1045931
48. Machado DT, Dias BDC, Cayô R, *et al.* Uncovering new *Firmicutes* species in vertebrate hosts through metagenome-assembled genomes with potential for sporulation. *Microbiol Spectr* 2024;**12**:e02113–24. https://doi.org/10.1128/spectrum.02113-24
49. Martin W, Russell MJ. On the origin of biochemistry at an alkaline hydrothermal vent. *Philos Trans R Soc B Biol Sci* 2007;**362**:1887–926. https://doi.org/10.1098/rstb.2006.1881
50. Fuchs G. Alternative pathways of carbon dioxide fixation: insights into the early evolution of life? *Ann Rev Microbiol* 2011;**65**:631–58. https://doi.org/10.1146/annurev-micro-090110-102801
51. Lane N, Martin WF. The origin of membrane bioenergetics. *Cell.* 2012;**151**:1406–16. https://doi.org/10.1016/j.cell.2012.11.050
52. Martin WF, Sousa FL, Lane N. Energy at life's origin. *Science.* 2014;**344**:1092–3. https://doi.org/10.1126/science.1251653
53. Colman DR, Kraus EA, Thieringer PH, *et al.* Deep-branching acetogens in serpentinized subsurface fluids of Oman. *Proc Natl Acad Sci* 2022;**119**:e2206845119. https://doi.org/10.1073/pnas.2206845119
54. Ragsdale SW. Enzymology of the Wood–Ljungdahl pathway of acetogenesis. *Ann N Y Acad Sci* 2008;**1125**:129–36. https://doi.org/10.1196/annals.1419.015
55. Shin J, Song Y, Jeong Y, *et al.* Analysis of the core genome and pan-genome of autotrophic acetogenic bacteria. *Front Microbiol* 2016;**7**:1531. https://doi.org/10.3389/fmicb.2016.01531
56. Sokolovskaya OM, Shelton AN, Taga ME. Sharing vitamins: cobamides unveil microbial interactions. *Science.* 2020;**369**:eaba0165. https://doi.org/10.1126/science.aba0165
57. Shelton AN, Seth EC, Mok KC, *et al.* Uneven distribution of cobamide biosynthesis and dependence in bacteria predicted by comparative genomics. *ISME J* 2019;**13**:789–804. https://doi.org/10.1038/s41396-018-0304-9
58. Brazelton WJ, McGonigle JM, Motamedi S, *et al.* Metabolic strategies shared by basement residents of the Lost City hydrothermal field. *Appl Environ Microbiol* 2022;**88**:e00929–22. https://doi.org/10.1128/aem.00929-22
59. Suzuki S, Ishii SI, Hoshino T, *et al.* Unusual metabolic diversity of hyperalkaliphilic microbial communities associated with subterranean serpentinization at The Cedars. *ISME J* 2017;**11**:2584–98. https://doi.org/10.1038/ismej.2017.111

Downloaded from academic.oup.com/ismecommun/article/6/1/ycag293/8907494 by NATIONAL INSTITUTE FOR MATERIALS SCIENCE user on 18 November 2026

© The Author(s) 2026. Published by Oxford University Press on behalf of the International Society for Microbial Ecology. This is an Open Access article distributed under the terms of the Creative Commons Attribution License (https://creativecommons.org/licenses/by/4.0/), which permits unrestricted reuse, distribution, and reproduction in any medium, provided the original work is properly cited.
ISME Communications, 2026, **6(1)**, ycag293
https://doi.org/10.1093/ismeco/ycag293
Original Article
Editor's Choice